Earth and Planetary Science Letters 622 (2023) 118408

Contents lists available at ScienceDirect

Earth and Planetary Science Letters

journal homepage: www.elsevier.com/locate/epsl

A shifty Toba magma reservoir: Improved eruption chronology and petrochronological evidence for lateral growth of a giant magma body

Dawid Szymanowski [a,b,*], Francesca Forni [c,d], Marcus Phua [d], Brian Jicha [e], Daniel W.J. Lee [d,f], Ying-Jui Hsu [d], Hamdi Rifai [g], Blair Schoene [b], Caroline Bouvet de Maisonneuve [d]

[a] Institute of Geochemistry and Petrology, ETH Zurich, 8092 Zurich, Switzerland
[b] Department of Geosciences, Princeton University, Princeton, NJ 08544, USA
[c] Dipartimento di Scienze della Terra "Ardito Desio", Università degli Studi di Milano, 20133 Milan, Italy
[d] Earth Observatory of Singapore and Asian School of the Environment, Nanyang Technological University, Singapore 639798, Singapore
[e] Department of Geoscience, University of Wisconsin-Madison, Madison, WI 53706, USA
[f] Lamont-Doherty Earth Observatory, Columbia University, Palisades, NY 10964, USA
[g] Department of Physics, Universitas Negeri Padang, Padang 25131, Indonesia

ARTICLE INFO

Article history:
Received 31 July 2023
Received in revised form 7 September 2023
Accepted 15 September 2023
Available online xxxx
Editor: C.M. Petrone

Keywords:
caldera collapse
magma reservoir
zircon crystallisation
U-Pb geochronology
Hafnium isotopes
40Ar/39Ar dating

ABSTRACT

Polycyclic caldera complexes hold clues to understanding why some magmatic systems develop into supersized magma bodies and how they can recover to produce several caldera-forming eruptions. However, the geologic records of the transitions between successive caldera events are very often inaccessible due to limited preservation of eruptive products of inter-caldera activity, prompting the search for alternative archives of magma evolution such as accessory minerals. Here we applied multiple geochemical tools to study one of the most active caldera centres of the Quaternary, the Toba caldera complex in Sumatra (Indonesia), which produced at least four caldera-forming eruptions in the last 1.6 My, including the iconic Youngest Toba Tuff at 74 ka. We combined feldspar $^{40}Ar/^{39}Ar$ and zircon U–Pb geochronology of proximal pyroclastic deposits with glass and mineral chemistry of both the tuffs and distal marine tephra to revise the eruption chronology of Toba, obtaining new eruption ages of 1417 -31/+14 ka (zircon) or 1339 ± 39/39 ka (plagioclase, internal/full external 2σ uncertainty) for the Haranggaol Dacite Tuff, 783.81 ± 0.85/1.32 ka (sanidine) for Oldest Toba Tuff, and 503.61 ± 1.36/1.50 ka (sanidine) for Middle Toba Tuff. Isotope dilution thermal ionisation mass spectrometry (ID-TIMS) U–Pb crystallisation ages, trace element contents and Hf isotopic ratios of zircons illuminate changes in the shallow magma reservoir which saw near-continuous zircon crystallisation over 1.6 My. Prolonged build-ups to each eruption with highly scattered zircon trace element compositions reflect a complex, heterogeneous character of the shallow reservoir, without a clear temporal trend or indications of the eruption trigger. In contrast, hafnium isotopes in zircon display a pronounced shift towards unradiogenic values immediately after the OTT caldera collapse, followed by a gradual recovery to a baseline value of $\varepsilon Hf = -7$ at the time of YTT eruption, interpreted as a reflection of the shift in magma reservoir position corresponding to change in the character of assimilated crust. We can show in unprecedented detail how a large caldera collapse affects magma geochemistry; however, identification of patterns in the behaviour of the Toba system and making geochemistry-based predictions about its future development remain a challenge.

1. Introduction

Silicic calderas pose a notable, if statistically rare, risk of explosive eruptions of magnitudes large enough to directly affect human activity hundreds of kilometres from the source and disperse volcanic ash and aerosols globally, possibly affecting short-term climate patterns (Black et al., 2021). The largest ('super') eruptions recur on timescales longer than modern human experience (Pyle, 1995; Mason et al., 2004), making the study of deposits of such events critical to the understanding of processes that lead to exceptionally large accumulations of eruptible magma. Studies of young calderas with well-exposed records of both caldera-forming

* Corresponding author.
E-mail address: dawid.szymanowski@erdw.ethz.ch (D. Szymanowski).

https://doi.org/10.1016/j.epsl.2023.118408

eruptions and any intervening activity suggest that such systems might undergo systematic changes in magma chemistry leading up to every massive eruption (Barker et al., 2015; Forni et al., 2018; Bouvet de Maisonneuve et al., 2021). However, today, many potentially active caldera systems are located in densely vegetated regions, limiting sampling to just the largest eruptive events.

One of such systems is Toba, Indonesia, one of the most productive caldera systems of the Quaternary and the source of the iconic Youngest Toba Tuff found as an ash layer across large swaths of the eastern hemisphere (Costa et al., 2014). Due to poor exposure in the proximal area, the known eruptive history of Toba is limited to little more than four large caldera-forming eruptions whose deposits are both difficult to distinguish in the field and uncharacteristic in whole-rock and glass compositions, leading to misidentifications (e.g. Ito, 2020) and disagreements about the eruption chronology (e.g. occurrence of two closely-spaced eruptions at ca. 790 ka, Mark et al., 2017). The absence of exposed deposits of inter-caldera activity at Toba has so far precluded a comprehensive model of the processes behind the build-up and successive reconstructions of the magma body. The most successful approach (predominantly focused on the latest Youngest Toba Tuff) utilised the accessory mineral (zircon, allanite) record of the large eruptions to constrain the length of time required for the magma build-up and to search for systematic changes in magma composition (Vazquez and Reid, 2004; Reid and Vazquez, 2017; Tierney et al., 2019; Liu et al., 2021). However, despite the geophysical inference of melt below the present-day caldera (Jaxybulatov et al., 2014), localised eruptive activity as recently as 55 ka, and continued resurgence (Mucek et al., 2017), clear patterns of behaviour of this supersized magma body are yet to emerge.

Here, in a step towards improving the understanding of Toba magmatism and the eventual appraisal of the present-day status of the system, we revise the eruptive chronology of this caldera centre and generate a detailed record of changes in magma chemistry over the last 1.6 My. We leverage improvements in sample preparation to generate a unique record of precise U–Pb zircon dates and compositions characterising the build-up to the four large explosive eruptions, which is then combined with new $^{40}Ar/^{39}Ar$ eruption ages as well as new and legacy chemical and isotopic compositions of bulk rocks, glasses and select minerals. We find near-continuous magmatic activity over the investigated timespan, with evidence of shifts in reservoir geometry but with a monotonous, buffered pattern of magma chemistry.

2. Geological setting

Toba caldera is located on the island of Sumatra in the westernmost branch of the Sunda volcanic arc (Fig. 1). Volcanic activity in this area results from the oblique subduction of the Indo-Australian oceanic plate beneath the Eurasian continental plate (Hamilton, 1979; Barber et al., 2005). Toba is the most productive magmatic system in the region, having generated at least four large caldera-forming eruptions in the last ca. 1.6 My (Knight et al., 1986; Chesner et al., 1991; Chesner and Rose, 1991): the Haranggaol Dacite Tuff (HDT; ~1.2 Ma), the Oldest Toba Tuff (OTT; ~790 ka), the Middle Toba Tuff (MTT; ~500 ka) and the Youngest Toba Tuff (YTT; 74 ka; Fig. 1A). Some authors have proposed that such exceptional magma productivity might be related to a significant increase of the angle of subduction below Toba and consequent slab tearing (Page et al., 1979), while others suggest that subduction of the Investigator Ridge Fracture Zone almost directly below Toba could favour volatile transfer into the mantle wedge thus enhancing melt production (Fauzi et al., 1996).

The most recent of the Toba eruptions, the YTT, formed the present caldera depression and is the largest known eruption of the Quaternary, with an estimated erupted volume of ~5300 km^3

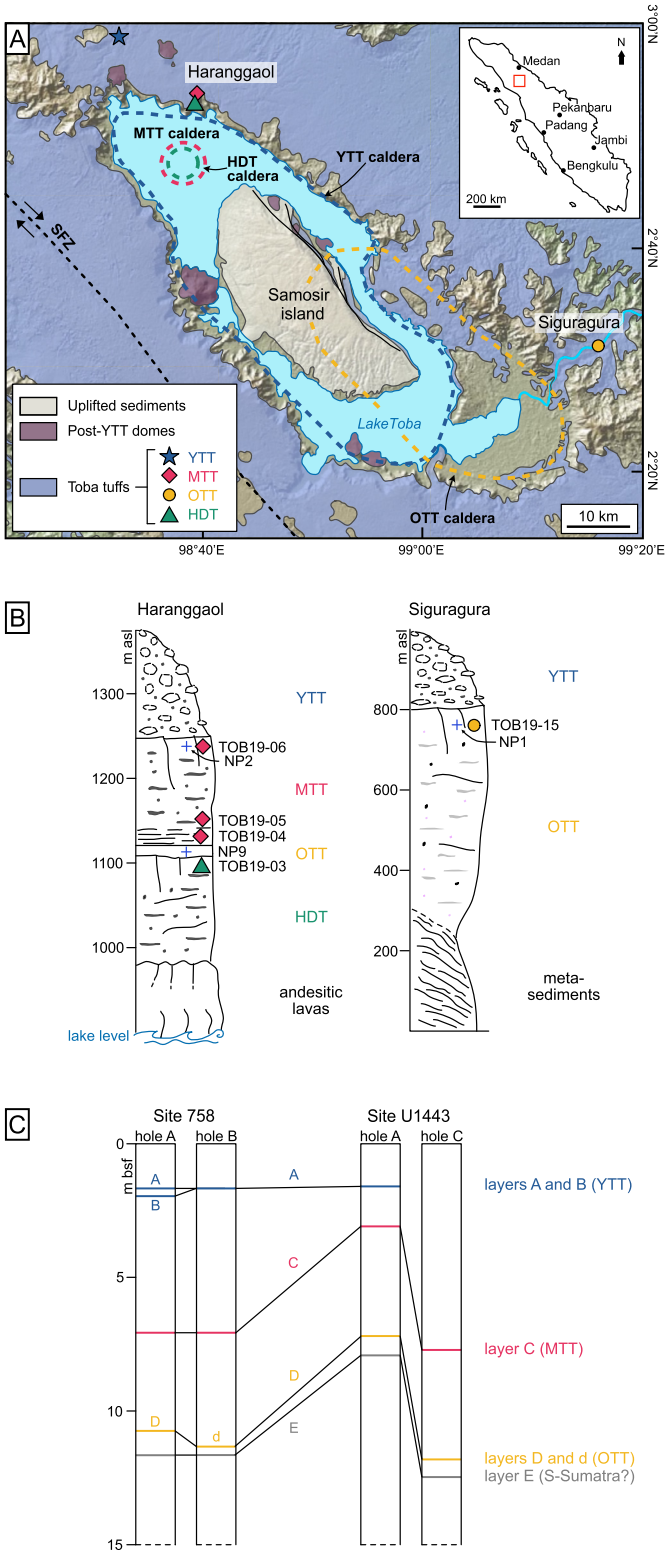

Fig. 1. Map of Toba caldera, northern Sumatra (A), schematic stratigraphic columns of two key sections of the Toba tuffs at Haranggaol and Siguragura (B), and stratigraphic position of major tephra layers in (I)ODP marine cores at sites 758 (holes A and B) and U1443 (C). Dashed lines in (A) indicate the source calderas of the four Toba tuffs as delineated by Chesner and Rose (1991). SFZ – Sumatra Fault Zone. Symbols in (A) and (B) represent sampling localities of HDT, OTT, MTT, and YTT for this study (TOB19*) while samples NP* are from Mark et al. (2017). Correlations in (C) are based on Dehn et al. (1991), Lee et al. (2004), Clemens et al. (2016), Bouvet de Maisonneuve and Bergal-Kuvikas (2020) and this work.

DRE (dense rock equivalent; Costa et al., 2014). The volumes and caldera footprints of the previous eruptions are not well constrained due to the paucity of outcrops in the heavily vegetated proximal areas, where older deposits are covered with hundreds of meters of YTT (Fig. 1A). The best section of Toba stratigraphy is exposed in the Haranggaol gully (NE sector of Toba), where the HDT rests upon andesitic lavas and is covered by the more recent ignimbrites (Fig. 1B). Based on the occurrence of HDT and MTT deposits only in the northern sector of the present-day caldera, Chesner and Rose (1991) hypothesised a source in the north of Toba for these two eruptions, while for OTT a source in the south is indicated by the presence of thick deposits in the area of Siguragura (SE sector of Toba). Distal ash deposits of Toba have been recognised hundreds to thousands of kilometres away from the source, representing excellent markers for stratigraphic correlations (e.g. Dehn et al., 1991; Lee et al., 2004; Smith et al., 2011; Mark et al., 2014; Kutterolf et al., 2023). Since the YTT eruption, a caldera lake has developed in the depression while the caldera floor experienced episodic uplift leading to the formation of the Samosir island (Fig. 1A). Geochronological data indicate that resurgence continued at least until ~2.7 ka and was accompanied by effusive activity (~70–55 ka) along the caldera rims and at the margins of Samosir (Mucek et al., 2017). The current state of the system has been assessed with ambient noise seismic tomography whose results are interpreted to indicate magma below 7 km depth, forming a crustal-scale sill complex centred below Samosir (Jaxybulatov et al., 2014).

The Toba tuffs are rhyolitic except for HDT which is dacitic in bulk-rock composition. The rhyolites contain up to 40% crystals of quartz, sanidine, plagioclase, amphibole, biotite, orthopyroxene and Fe-Ti oxides with accessory zircon, allanite, fayalite and apatite, while HDT contains a similar fraction of plagioclase, two pyroxenes, Fe-Ti oxides, apatite, and zircon (Chesner, 1998). Zircon and allanite ages, previously used to constrain the duration of magma assembly at Toba, indicate protracted crystallisation of these accessory mineral phases for hundreds of thousands of years before each rhyolite eruption, with limited evidence of secular chemical evolution (Vazquez and Reid, 2004; Reid and Vazquez, 2017; Tierney et al., 2019; Ito, 2020; Liu et al., 2021).

3. Samples and methods

We studied five representative samples of the four caldera-forming eruptions of Toba (HDT, OTT, MTT, YTT) from two classic outcrops (Fig. 1A, B), with an additional sample collected at Haranggaol aimed at identifying the OTT reported there by Mark et al. (2017). To better reconstruct the eruptive history of Toba, we also sampled volcanic glass from ash layers recovered from IODP Site U1443 core (Clemens et al., 2016), drilled ca. 1000 km NW of Toba on the Ninetyeast Ridge in the Indian Ocean, about 100 m from ODP Site 758 which had been used previously as the main reference for distal Toba tephra (Fig. 1C; Dehn et al., 1991). To confirm unit identification and obtain storage pressure estimates, we analysed glass, biotite, and amphibole major element compositions by electron microprobe at Nanyang Technological University, Singapore. $^{40}Ar/^{39}Ar$ single crystal fusions of sanidine (MTT, OTT) and plagioclase (HDT) were performed at University of Wisconsin-Madison following the methods of Jicha et al. (2016). For zircon petrochronology, we selected 15–30 large crystals per eruptive unit (Fig. S1) to maximise the amount of radiogenic Pb available for analysis. U–Pb isotopes in single zircon crystals were analysed by isotope dilution thermal ionisation mass spectrometry (ID-TIMS) at Princeton University following the methods of Schoene et al. (2019). $^{206}Pb/^{238}U$ dates were corrected for $^{230}Th/^{238}U$ disequilibrium using a modified correction scheme appropriate for young samples that may not have returned to secular equilibrium (Sakata et al., 2017). Common Pb exceeding the amount expected from lab processing (100 fg) was likely sourced from ubiquitous melt and apatite inclusions in zircon and was corrected for with a composition derived from independent TIMS analyses of Pb isotopes in feldspars separated from the respective samples (Fig. S2). Following U–Pb geochronology of zircon, we used the remaining solutions of matrix elements to analyse elemental compositions and Hf isotope ratios following methods described in O'Connor et al. (2022). Analytical methods and results are detailed in the Supplementary material and Table S1.

4. Results

4.1. Glass and biotite geochemistry

We analysed major element compositions of glass shards from ash layers sampled within holes A and C of Site U1443, as well as matrix glass and biotite from the proximal tuffs, and compared the compositions to existing data from Site 758 and on-land samples (Dehn et al., 1991; Smith et al., 2011; Mark et al., 2017; Pearce et al., 2020). HDT matrix glasses are rhyolitic, with similar K_2O and lower SiO_2 contents than OTT, MTT, and YTT (Fig. 2A). Similar to Smith et al. (2011), we found that matrix glasses from the three younger tuffs fully overlap in major element composition, while biotite crystals record compositional differences (e.g. in FeO/MgO ratios and MnO concentrations) that allow clear distinction between these units. The compositions of biotite from our samples closely match those from the literature, supporting our unit assignments and extending the field of MTT biotite towards higher FeO/MgO values (Fig. 2B). In the marine record (Fig. 1C), previous work on Site 758 has identified multiple Quaternary tephra layers (from A to M in increasing age order; Dehn et al., 1991), some of which were correlated to Toba units YTT (A, B), MTT (C), OTT (D, d), and HDT (F; Dehn et al., 1991; Bouvet de Maisonneuve and Bergal-Kuvikas, 2020). Glass compositions allow identification of ash layers equivalent to MTT and OTT among tephra recovered at Site U1443 (Fig. 2A), confirming the existing correlations (Clemens et al., 2016). However, we found no evidence for an additional layer (d) located between levels D and E, which would correspond to the first of the proposed two OTT eruptions of Mark et al. (2017). Finally, we can confirm that glass shards from layer E do not correspond to proximal HDT and they have a different geochemical affinity compared to the Toba tuffs (Bouvet de Maisonneuve and Bergal-Kuvikas, 2020).

4.2. $^{40}Ar/^{39}Ar$ eruption ages

We obtained three new high-precision sanidine $^{40}Ar/^{39}Ar$ ages including two for MTT (samples TOB19-04 and 05 from Haranggaol) and one for OTT (TOB19-15 at Siguragura), as well as a plagioclase age for HDT (TOB19-03 at Haranggaol; Fig. 3). The results for sanidine display a spread of individual dates beyond that expected from a single, eruption-age population, as increasingly seen in single-crystal sanidine $^{40}Ar/^{39}Ar$ datasets (e.g. Rivera et al., 2014; Andersen et al., 2017; Mucek et al., 2021). Using the Bayesian approach to eruption age interpretation (Keller et al., 2018) results in overlapping ages for the two samples of MTT, and a combined age of 503.61 ± 1.36/1.50 ka (internal/full external 2σ uncertainty), marginally older than the age obtained by Mark et al. (2017; Fig. S3). OTT at Siguragura similarly yielded a range of dates of ca. 10 ky; our new Bayesian age of 783.81 ± 0.85/1.32 ka is consistent with the data of Mark et al. (2017), with all new data plotting well within the spread of their individual dates obtained at two localities (Fig. S3). HDT contains no sanidine; results obtained from four out of 12 plagioclases with highest K contents yielded a Bayesian age of 1339 ± 39/39 ka, similar to the frequently quoted age of 1.2–1.3 Ma (Nishimura et al., 1984) but significantly younger

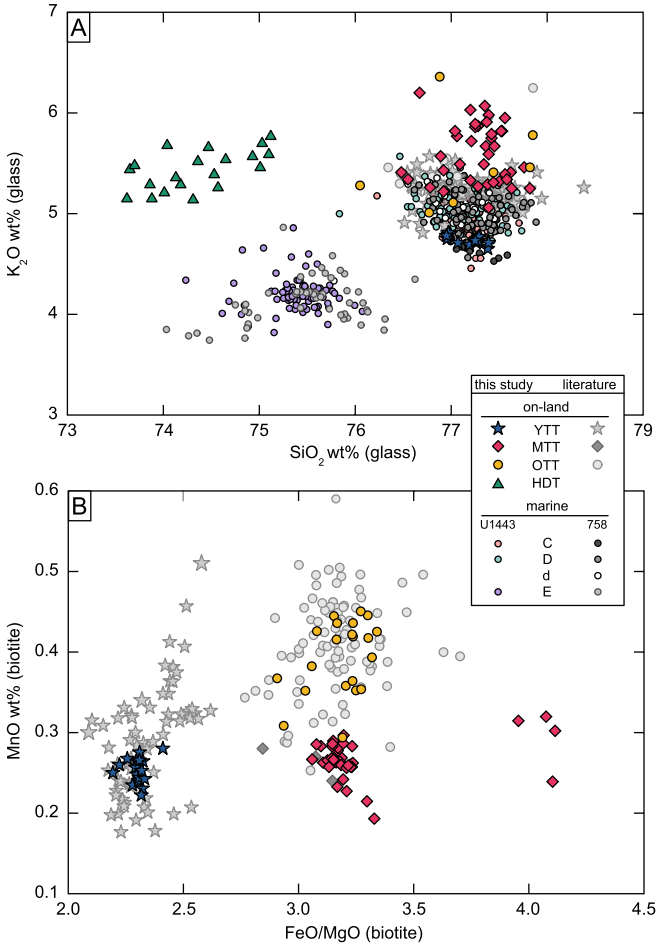

Fig. 2. Major element compositions of glass (A) and biotite (B) from proximal Toba tuffs and the marine cores. Glass data are from this study and Chesner and Luhr (2010), Smith et al. (2011), and Mark et al. (2017). Biotite data (proximal tuffs only) are from this study and Smith et al. (2011).

than HDT zircon crystallisation ages presented here and by Liu et al. (2021).

4.3. Zircon $^{206}Pb/^{238}U$ crystallisation ages

U–Pb geochronology on 102 zircon crystals from the four eruptions (Table S1) returned dispersed zircon $^{206}Pb/^{238}U$ dates that are in every case older than the corresponding $^{40}Ar/^{39}Ar$ feldspar eruption age (Fig. 4) and are considered representative of the range of single zircon crystallisation ages. We found little inheritance of whole zircons with ages fitting in the age range of previous caldera-forming events (one crystal each for MTT and OTT within YTT). This is similar to the results of previous studies finding limited inheritance from preceding magma build-ups (Reid and Vazquez, 2017; Ito, 2020; Liu et al., 2021) and an effect likely compounded by the greater age-averaging potential of the whole-crystal ID-TIMS technique in comparison to *in situ* dates. Our ages have similar distributions to those in previous studies of Toba zircon (Figs. S4-5). However, because of both the differences in analytical volume (whole crystal vs. surface/smaller inner domain) and the size bias of large crystals studied here, except for MTT we did not recover truly *eruption age* zircons (i.e. overlapping the $^{40}Ar/^{39}Ar$ eruption age; cf. Tierney et al., 2019). Excluding clear xenocrysts, the apparent minimum time of pre-eruptive zircon crystallisation described by our ages (calculated following Klein and Eddy, 2023) ranges from ca. 140 ky for the smaller HDT and MTT to over 400 ky for OTT (Table 1). Several crystals from all four units returned discordant dates with upper intercept ages indicative of the inclusion of old xenocrystic cores ranging in age between ca. 340 and 1480 Ma (Fig. S1), extending the array of (dominantly core) *in situ* U–Pb ages reaching 650 Ma (Reid and Vazquez, 2017; Liu et al., 2021). The presence of xenocrystic domains that are up to Proterozoic in age is a clear indication of the involvement of old crust in petrogenesis of the Toba tuffs.

4.4. Zircon trace elements

Elemental compositions obtained from bulk zircon crystals reveal a large range of trace element contents in the three younger eruptions, and a limited variability in HDT zircons (Fig. 5). Element co-variation trends are clear and correspond well to the observed mineralogy of the Toba tuffs. Variations in Zr/Hf, which tends to track zircon crystallisation, are strongly correlated with changes in Eu/Eu^* tracking feldspars (high D_{Eu} compared to D_{Sm} and D_{Gd}), Yb/Gd – allanite (low $D_{Yb/Gd}$), as well as with incompatible elements such as Nb. This suggests that the majority of Toba zircons crystallised from variably evolved melts saturated in feldspars and allanite, likely in addition to quartz, biotite, amphibole, apatite, and Fe-Ti oxides that have comparably low leverage on zircon compositions (e.g. Padilla and Gualda, 2016). While the whole-crystal trace elements in the three tuffs show clear co-variation trends, they do not display any systematics with time (Fig. 4), likely reflecting heterogeneous magma bodies characterised by the coexistence of melts of different temperature and degree of magma evolution. Our results are consistent with the limited literature data for OTT and MTT (Liu et al., 2021). The case of YTT, where the most

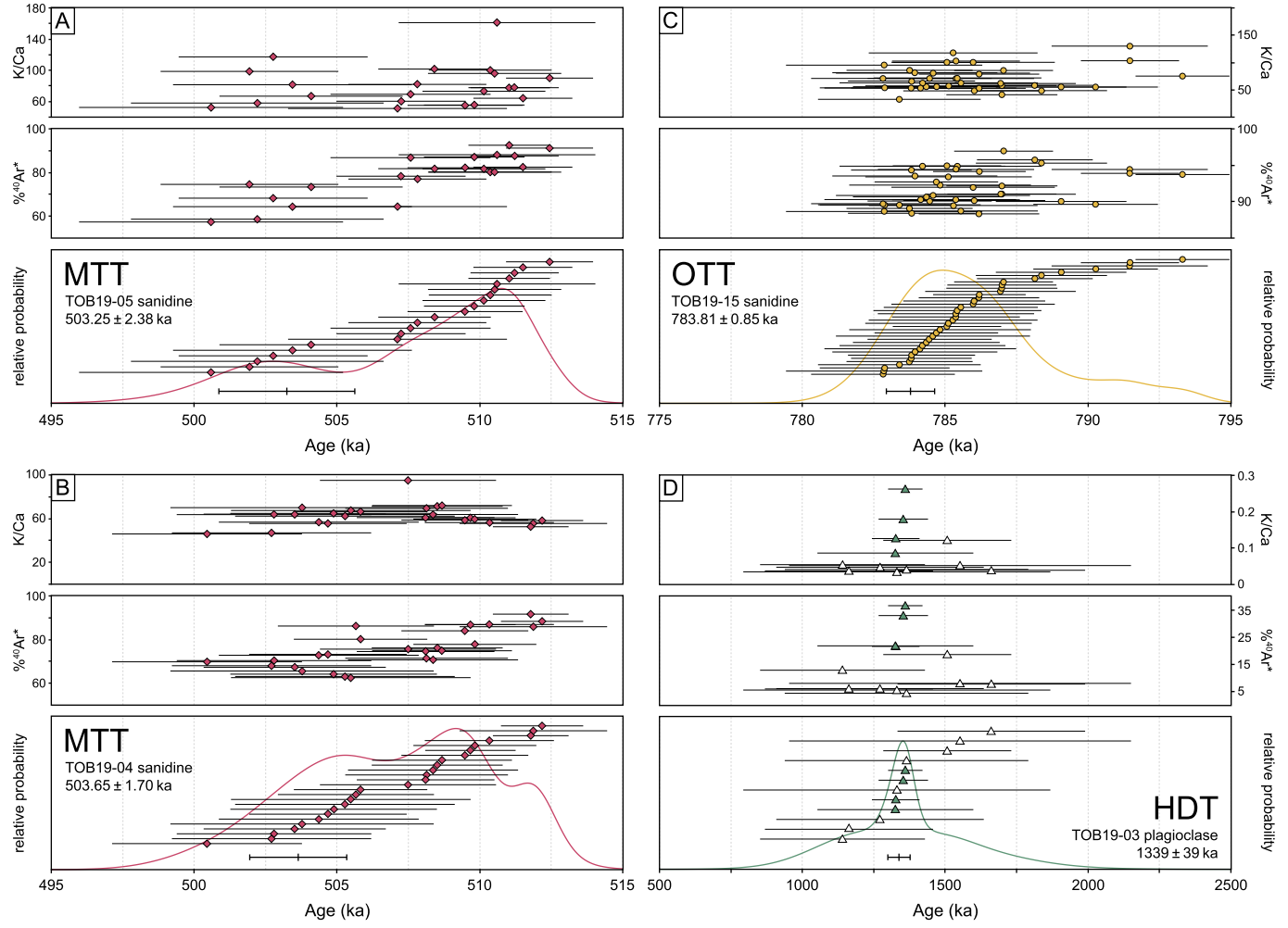

Fig. 3. $^{40}Ar/^{39}Ar$ feldspar geochronology of the Toba tuffs: MTT (A, B), OTT (C), and HDT (D). %Ar* – percent radiogenic Ar. Eruption ages were estimated using the Bayesian model of Keller et al. (2018) with an exponential prior distribution, using all data (MTT, OTT) or only data with >20% Ar* (HDT). The two MTT samples are combined to calculate a best-estimate MTT age in Table 1. All error bars represent 2σ analytical uncertainties.

Table 1
Eruption age estimates for the Toba tuffs.

Unit	$^{40}Ar/^{39}Ar$			$^{206}Pb/^{238}U$				Minimum zircon crystallisation timescale (ky)
	Bayesian age (ka)	2σ int	2σ ext	youngest zircon age (ka)	2σ	Bayesian age (ka)	95% CI	
Youngest Toba Tuff (YTT)	**73.8***	**0.6**	**0.8**	107	7	92	+13/-29	333
Middle Toba Tuff (MTT)	**503.61**	**1.36**	**1.50**	514	20	523	+12/-16	140
Oldest Toba Tuff (OTT)	**783.81**	**0.85**	**1.32**	808	7	803	+11/-26	411
Haranggaol Dacite Tuff (HDT)	1339.3	38.7	38.8	1428	7	**1417**	**+14/-31**	143

Bayesian ages estimated following Keller et al. (2018) using a truncated normal prior distribution and excluding xenocrysts (U-Pb zircon), or using an exponential prior and all dates with >20% Ar* ($^{40}Ar/^{39}Ar$ feldspar).
$^{40}Ar/^{39}Ar$ ages calculated relative to ACs at 1.1864 Ma (Jicha et al., 2016) and the decay constants of Min et al. (2000). Internal uncertainty (int) represents the uncertainty of the Bayesian estimate using analytical results only; external uncertainty (ext) also includes uncertainties associated with the age of the monitor mineral and decay constant uncertainties. *YTT $^{40}Ar/^{39}Ar$ age recalculated from Mark et al. (2017).
All U-Pb ages are presented with internal analytical uncertainties; contributions of tracer calibration and decay constant uncertainty are negligible.
Minimum zircon crystallisation timescales are calculated following Klein and Eddy (2023).
Preferred eruption age estimates are shown in bold.

data are available (Tierney et al., 2019; Liu et al., 2021), provides a unique comparison of bulk-zircon and *in situ* compositions and ages; bulk compositions apparently under-sample the true compositional variability, while the youngest, eruption-age zircon surfaces display some of the most evolved compositions (Figs. 4, S6). HDT zircons are homogeneous at single-crystal scale and compositionally unevolved, suggesting distinct zircon crystallisation conditions from a low-crystallinity magma that did not saturate in allanite, consistent with the observed mineralogy.

4.5. Radiogenic isotopes

Initial radiogenic Hf isotope ratios of the dated zircons vary between εHf of -11 and -6 relative to the model chondritic composition (CHUR; Bouvier et al., 2008) and display a clear trend with time over ca. 600 ky prior to the YTT eruption (Fig. 6A). εHf in zircons and, consequently, in their parental melts, was invariable throughout HDT and OTT magma accumulation at ca. -7 to -8, followed by a shift recorded by all but one MTT zircon to ca. -10. All subsequent values recorded by MTT and YTT zircons sys-

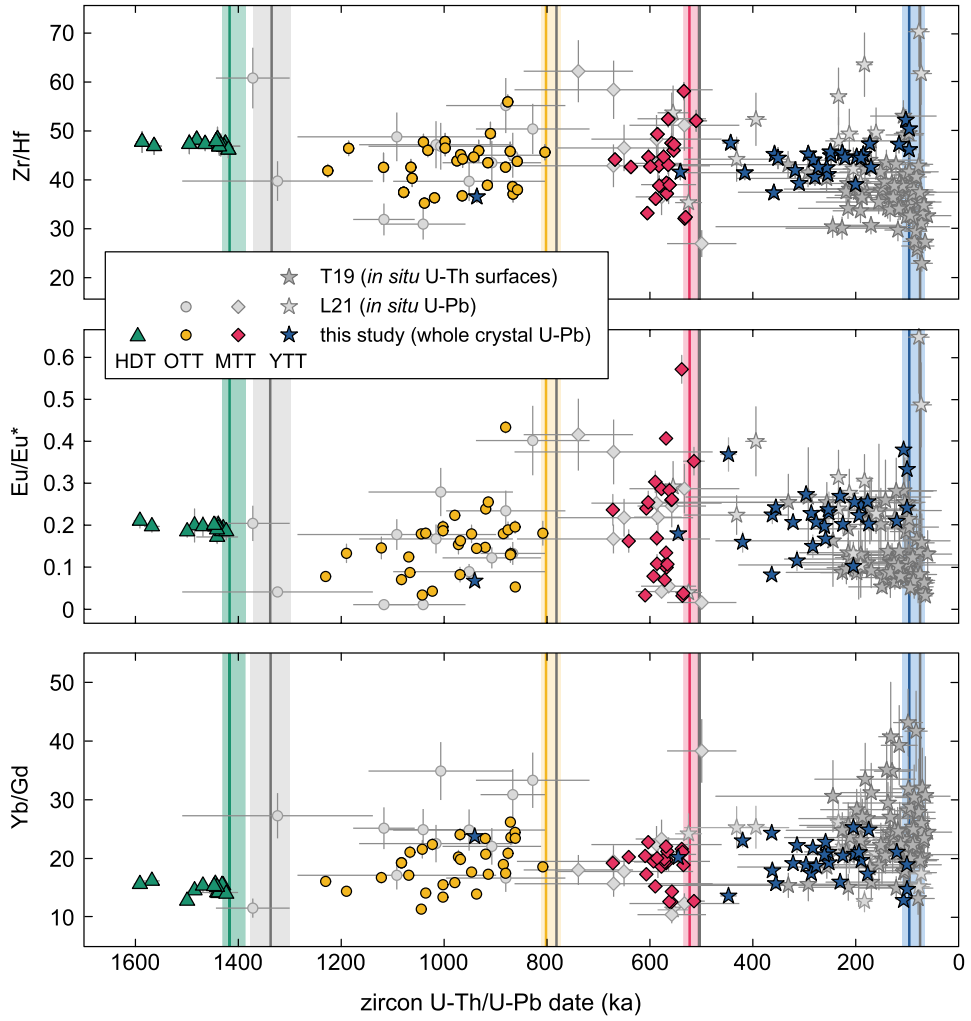

Fig. 4. Zircon dates and compositions in caldera-forming Toba tuffs. Whole-crystal ID-TIMS $^{206}Pb/^{238}U$ dates and corresponding whole-crystal compositions from this study (coloured symbols) are shown with *in situ* $^{206}Pb/^{238}U$ dates and compositions of crystal cores and rims from Liu et al. (2021; L21) and $^{230}Th/^{238}U$ disequilibrium dates and compositions of YTT zircon surfaces from Tierney et al. (2019; T19). Vertical lines and shaded 95% confidence intervals corresponding in colour to the zircon symbols from each tuff indicate the zircon-based Bayesian U-Pb eruption age estimate, while grey lines indicate the Bayesian $^{40}Ar/^{39}Ar$ eruption age estimate for each unit (both age interpretations following Keller et al., 2018). Data-point error bars represent 2σ analytical uncertainties.

tematically increase to reach the original εHf of -7 at the time of YTT eruption. Since some YTT zircons have been shown to contain MTT-aged cores (Reid and Vazquez, 2017), the MTT-YTT array could be thought to result from mixing of young, relatively radiogenic outer zones with older, less radiogenic cores. However, not all YTT zircon surfaces are eruption-aged (Tierney et al., 2019; Fig. 4), so the trend cannot be a simple two-component mixing line but rather a temporal progression in εHf that may be additionally smoothed by analytical mixing effects. This is confirmed by recent *in situ* Hf isotopic data of Liu et al. (2022a) suggesting a similar trend. The offset of MTT magmas to a less radiogenic εHf is mirrored by literature data for Sr isotopes (Chesner, 1988; Jones, 1993; Turner and Foden, 2001; Budd et al., 2017), where initial $^{87}Sr/^{86}Sr$ of bulk rocks at time of eruption (Fig. 6B) are distinctly higher in MTT (0.7147–0.7153) than in the other three tuffs (mostly 0.7134–0.7140). Additionally, Chesner (1988) describes crystal–glass $^{87}Sr/^{86}Sr$ disequilibrium in YTT, indicating the same direction of progression as our εHf data i.e. towards more juvenile compositions.

4.6. Barometry

To constrain the depths of magma storage at Toba we used the amphibole barometer of Médard and Le Pennec (2022) suitable to silicic systems where amphibole is in equilibrium with plagioclase and biotite. Such a mineral assemblage closely matches that of OTT, MTT and YTT, but not HDT which lacks both amphibole and biotite. For barometric calculations we exclusively used amphibole compositions that satisfied the amphibole–melt equilibrium test of Putirka (2016). Our estimates indicate no clear pressure difference between OTT (1.8–2.7 kbar), MTT (1.5–3.5 kbar), and YTT (1.0–2.1 kbar; Fig. 6C), and are consistent with the results of Chesner and Luhr (2010) using melt inclusion barometry. The inferred pressure interval corresponds to a depth range of 4–13 km, consistent with typical magma storage depths found for large silicic reservoirs (Huber et al., 2019). The melt–phase assemblage machine learning-based barometer of Weber and Blundy (2023) returns similar pressure ranges for OTT, MTT and YTT and suggests a deeper storage (>3 kbar) for the HDT magma.

5. Discussion

5.1. Toba stratigraphy, eruption ages, and correlations to marine cores

5.1.1. Haranggaol stratigraphy

We revisited one of the few classic outcrops of Toba tuffs at Haranggaol (Fig. 1B). The section, as described originally (Knight et al., 1986), begins with andesitic lavas, followed by thick HDT, MTT

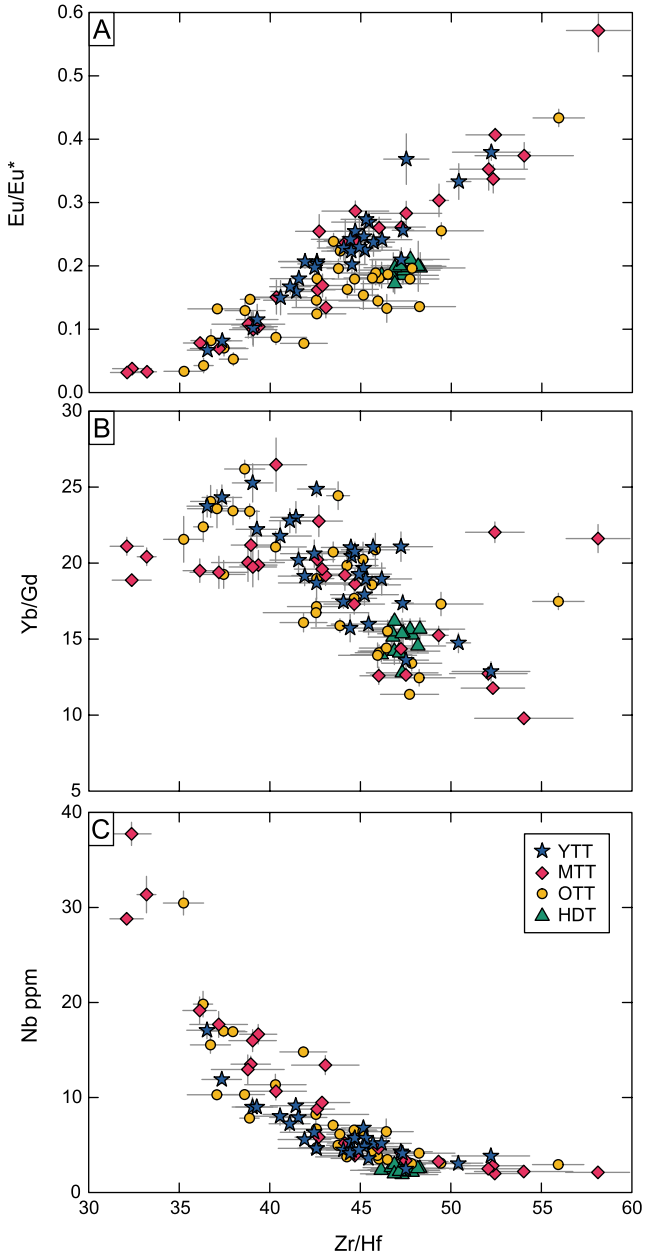

Fig. 5. Whole-crystal zircon element co-variations between Zr/Hf and Eu/Eu* (A), Yb/Gd (B), and Nb (C), shown with 2σ analytical uncertainties.

with a basal glassy section (i.e. basal vitrophyre), and is capped by about 100 m of YTT. However, the transition between HDT and MTT at Haranggaol, and the thicknesses of both units, have been controversial since Mark et al. (2017) obtained a $^{40}Ar/^{39}Ar$ sanidine age of 785.7 ± 1.4 ka (their sample NP9, Fig. 1B) within what used to be considered MTT, prompting the authors to assign a thick part of the section to a variety of OTT (OTT 'B'). We attempted to locate OTT in the section but only found MTT as low as 1120 m a.s.l. (sample TOB19-04 hereafter included in discussion as part of MTT). We also sampled HDT at an altitude of 1109 m a.s.l., which necessitates a substantial revision of the stratigraphic section (Fig. 1B), expanding the known thickness of HDT to some 120 m and implying that the magnitude of the HDT eruption might have been larger than previously thought. Our observations are permissive of there being a maximum of 11 m of OTT in this section between 1109 and 1120 m a.s.l. (cf. Mark et al., 2017), although we were not able to identify it directly. The reduced thickness of OTT at Haranggaol is consistent with the descriptions of Chesner and Rose (1991) who indicated near-absence of OTT in the NE sector of Toba.

5.1.2. Eruption ages of Toba tuffs

The new Bayesian $^{40}Ar/^{39}Ar$ age for the HDT is 1339 ± 39/39 ka, whereas the Bayesian zircon age based on our new ID-TIMS data is 1417 -31/+14 ka (Table 1, Fig. S5). Both new ages are within uncertainty of the K–Ar (1.3 ± 0.4 Ma) and fission track (1.2 ± 0.3 Ma) ages of Nishimura et al. (1984). However, only four of the twelve $^{40}Ar/^{39}Ar$ plagioclase dates come from crystals with K/Ca >0.1, so any age interpretation based on these $^{40}Ar/^{39}Ar$ data should be treated as preliminary. Consequently, we consider the U–Pb zircon dates to provide a more robust estimate of the HDT eruption age.

Our new eruption age for the OTT of 783.81 ± 0.85 ka is within uncertainty of the Mark et al. (2017) OTT 'B' age of 784.0 ± 1.2 ka (2σ; recalculated using same monitor age and decay constant used herein). It is worth noting that the range in dates exhibited by the Haranggaol OTT 'B' sample in Mark et al. (2017) fall entirely within the range in dates of their OTT 'A' sample from Siguragura (Fig. S3). We suggest that the less precise data of Mark et al. (2017) may be masking age dispersion due to Ar loss, excess Ar, or the presence of antecrysts in their OTT samples. The youngest 50 MTT dates of Mark et al. (2017) range from 490 to 510 ka and yield a weighted mean of 500.8 ± 1.2 ka (2σ; recalculated). Our new, multi-collector $^{40}Ar/^{39}Ar$ data are more precise and also show a more restricted range in dates from 500 to 512 ka (Fig. 3, S3), yielding a combined Bayesian eruption age estimate of 503.61 ± 1.36 ka. Given the smaller analytical uncertainties, we prefer our new $^{40}Ar/^{39}Ar$ ages as the most reliable eruption age estimates for OTT and MTT.

5.1.3. One OTT in marine cores and in the proximal record

Based on new geochronology and geochemical data from both the proximal tuffs and distal marine tephra layers, we can now revisit the eruptive history of Toba. While little doubt remains about the youngest large eruptions of YTT and MTT, recently Mark et al. (2017) have suggested the occurrence of two separate OTT eruptions, OTT 'A' and OTT 'B', at 792 and 786 ka. Their proposal was based on 1) the 6 ka difference in sanidine $^{40}Ar/^{39}Ar$ ages obtained for OTT samples NP1 and NP9 (Fig. 1B), and 2) the assumption that the two stratigraphically offset marine tephra D and d in Site 758 cores (holes A and B, respectively, Fig. 1C), both previously correlated to OTT (Dehn et al., 1991; Lee et al., 2004), represent separate eruptive events producing volcanic glass of identical composition. We question the validity of this proposal. Given the new multi-collector $^{40}Ar/^{39}Ar$ data and their comparison to the results of Mark et al. (2017; Fig. S3), we do not find sufficient geochronological evidence to argue for two closely spaced eruptions. Secondly, the idea of layers D and d representing distinct events is difficult to verify since they were only recovered as unique tephra layers in two separate holes (758A and 758B, Fig. 1C) from Site 758 that largely achieved full core recovery over the depth interval in question (Dehn et al., 1991). There is a slight difference in depth between layer D in hole 758A and layer d in hole 758B but, considering their identical composition and absence of other candidate correlative layers, Dehn et al. (1991) concluded that "d is possibly diffused or reworked tephra D". This is now supported by the recovery of a single layer D of indistinguishable composition 100 m away at Site U1443 (Fig. 1C, 2A), as well as at several other Indian Ocean drill sites (Kutterolf et al., 2023). Stratigraphically below layer D at Site U1443 we identified a distinct ash layer with glass compositions equivalent to layer E at Site 758 (Fig. 2A), representing an eruption which has yet to be identified but possibly originating from a separate volcanic centre e.g. in south Sumatra (Bouvet de Maisonneuve and Bergal-Kuvikas, 2020). Considering

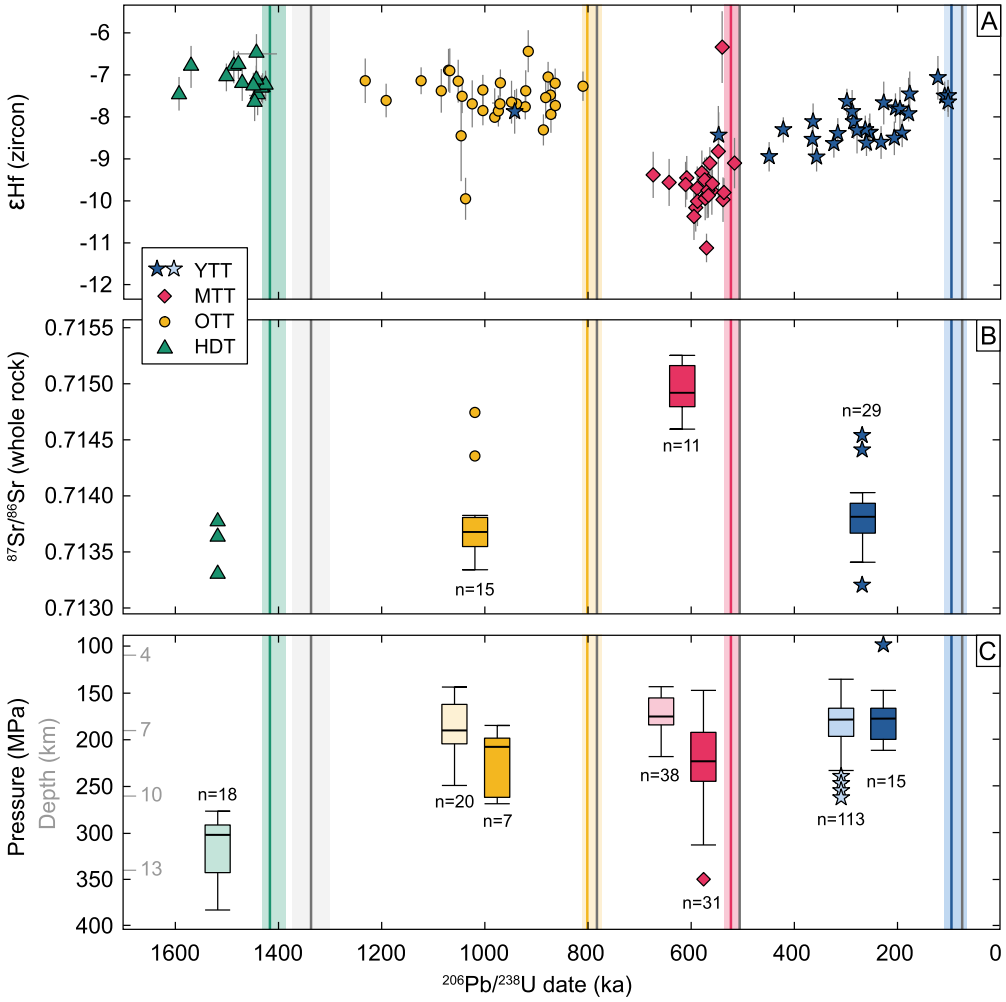

Fig. 6. Variability of radiogenic isotope compositions (A: Hf, B: Sr) and storage pressure estimates (C) in the Toba tuffs. A. Radiogenic Hf isotopes in zircon vs. ID-TIMS $^{206}Pb/^{238}U$ date. εHf is the deviation of initial $^{176}Hf/^{177}Hf$ from the chondritic uniform reservoir (CHUR; Bouvier et al., 2008) model composition in parts per 10,000. All uncertainties are 2σ. B. Compiled initial bulk-rock $^{87}Sr/^{86}Sr$ values from Chesner (1988), Jones (1993), Turner and Foden (2001), Budd et al. (2017), and Liu et al. (2022b). C. Magma storage pressures estimated using amphibole barometry (saturated colour; Médard and Le Pennec, 2022) and machine learning-based melt barometry (pale fill; Weber and Blundy, 2023). Corresponding crustal depths are calculated using a crustal density of 2700 kg/m^3. Boxes represent data from 1st to 3rd quartile (interquartile range, IR), with the median indicated by a line, while whiskers extend to minimum and maximum values (except if >1.5 IR away). Eruption ages are presented as in Fig. 4. Note that pressure estimates and bulk-rock Sr isotopes (B, C) do not carry an absolute age significance as zircon compositions do; they likely reflect the conditions at the time of each eruption.

both the geochronologic and stratigraphic arguments, we therefore find no evidence to support the idea of two OTT eruptions occurring 6 ky apart. In the following discussion, we thus refer to only one OTT event.

5.2. Evolution of the Toba magma supply system

5.2.1. Isotope signatures and melt sources

The four voluminous Toba tuffs are characterised by enriched isotopic values in O ($\delta^{18}O_{melt}$ = 6–10), Hf (εHf = -11 to -6), Nd (εNd = -11 to -8), and Sr ($^{87}Sr/^{86}Sr$ = 0.713–0.715; Chesner, 1988; Budd et al., 2017; Liu et al., 2022a,b) requiring a partial involvement of old crustal sources and mass contribution from materials that interacted with meteoric water. However, understanding where exactly in the melt supply chain these contributions occurred presents a challenge due to the absence of exposed mafic volcanic products that would be coeval and cogenetic with the tuffs. The closest approximation of parental Toba magmas comes from either the least evolved, post-YTT dome lavas (Fig. 1A) or the pre-HDT Haranggaol Andesite (HA), both of which are already enriched in trace elements and have fairly crustal isotopic compositions (Chesner, 1988; Jones, 1993; Turner and Foden, 2001; Mucek et al., 2017; Liu et al., 2022b). The least radiogenic of the post-YTT domes has $^{87}Sr/^{86}Sr$ = 0.7107 (Mucek et al., 2017) while the HA is 0.7122 (Liu et al., 2022b), suggesting that incorporation of the enriched materials into Toba melts occurred fairly deep in the magma plumbing system. Two main mechanisms have been proposed to explain the isotopic signatures: 1) assimilation within the continental crust, and 2) enrichment of the mantle source involving subducted sediments. The crustal architecture of Sumatra is relatively poorly understood since the continental crust represents a complex patchwork of terranes, including Palaeozoic and Mesozoic magmatic and metamorphic lithologies, as well as products of magmatic arc activity at least since the Triassic (Barber et al., 2005). No Precambrian basement has been reported in outcrops, but both xenocrysts as old as 1480 Ma in the Toba tuffs (this study and Reid and Vazquez, 2017; Liu et al., 2021), and xenocrysts found in younger, post-caldera basalts and andesites around Toba (up to 1640 Ma; Gao et al., 2022) testify to the presence of materials of this age in the crustal column. Evidently, there are materials in the Sumatran crust with the right characteristics to explain the isotopic signatures via crustal assimilation (Gasparon and Varne, 1998). The other end-member explanation calls upon enrichment

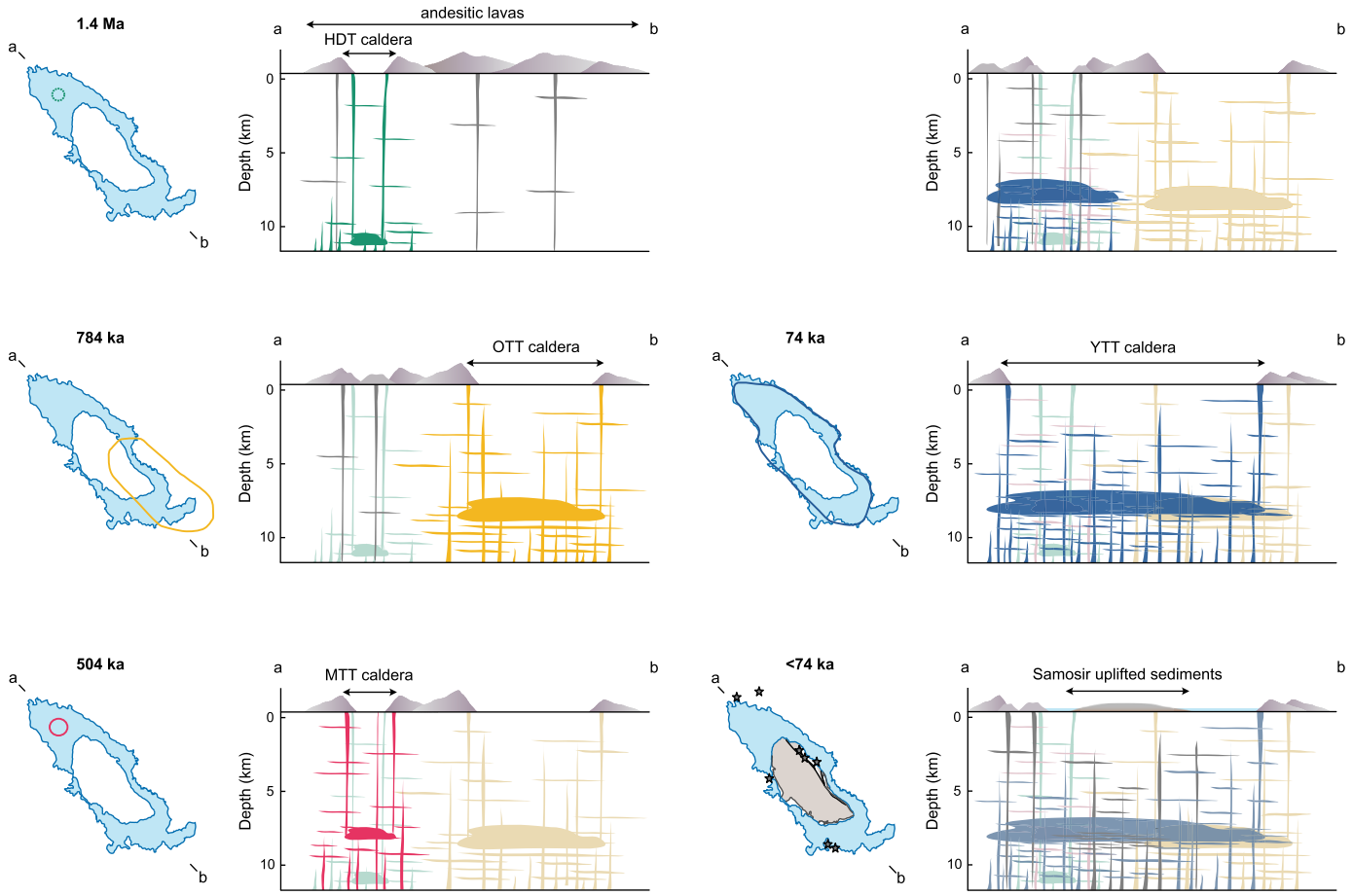

Fig. 7. Evolution of the magma reservoir beneath the Toba caldera complex. HDT reservoir developed in the NW sector, likely deeper (>3 kbar) than subsequent magma storage zones. The reservoir evacuated to form OTT accumulated in the SE sector, resulting in the formation of the OTT ('Porsea') caldera. In the period following OTT caldera collapse, new magma accumulated in the NW, interacting with crustal lithologies that had not been substantially modified by magmatism, leading to initially high-$^{87}Sr/^{86}Sr$, high-$\delta^{18}O$, low-εHf melts that were preferentially sampled by the eruption of MTT. Over time, the magma reservoir increased its lateral footprint towards the SE to reach its maximum extent prior to YTT eruption, while the decreasing importance of older crust in the mass balance of assimilation gradually shifted the isotopic signature towards values in line with the baseline values of Toba tuffs. Expressions of post-YTT activity include the extrusion of andesitic to rhyolitic domes (stars) and resurgent uplift of the Samosir area. Ages correspond to the preferred eruption age estimates from Table 1.

of the mantle source through addition of material derived from the particularly isotopically enriched subducted sediments of the Nicobar Fan accumulated offshore northern Sumatra since the Miocene (Gao et al., 2022; Liu et al., 2022b). Overall, while crustal assimilation appears the more viable mechanism for the Toba area (Gasparon and Varne, 1998; Turner and Foden, 2001), conclusive answers are precluded by the poor understanding of crustal lithologies and the fact that subducted continent-derived sediments are geochemically indistinguishable from the continental crust itself. Regardless, the remarkable homogeneity of the baseline isotopic composition of the Toba tuffs ($^{87}Sr/^{86}Sr = 0.7135$ and $\varepsilon Hf = -7$, Fig. 6) suggests that this signature is acquired deeper than the ca. 2 kbar storage level or it is efficiently buffered in the mature magma reservoir. In particular, the baseline isotopic signature is already present in HDT which was stored at >3 kbar. Smaller adjustments to the isotopic character of the melts are likely made within the upper crust as a function of magma reservoir geometry and eruptive history. It is these smaller adjustments (Fig. 6) that our high-precision U–Pb–Hf data reveal for the first time.

5.2.2. Shifts in reservoir location and geometry

The clear temporal changes in εHf resolved by the zircon petrochronology results (Fig. 6) allow us to track shallow magma reservoir dynamics in unprecedented detail. The baseline value of εHf =-7 seen in HDT and OTT was abruptly modified at the time of the OTT caldera collapse at 784 ka, after which a gradual recovery is observed over at least 600 ky leading to the YTT eruption. The temporal association between the shift in isotopic ratios, and both the OTT caldera collapse and the change in the location of the magma reservoir (Fig. 1A) may be coincidental, but except for earthquakes, few if any geological processes that could affect a magma plumbing system operate on the short timescale necessary to explain the observations. In particular, studies using zircon εHf have shown that changes of comparable magnitude due to variations in the degree of crustal assimilation occur over longer, million-year timescales (e.g. Schaltegger et al., 2019; Storck et al., 2020).

Significantly for isotopic ratios, a caldera collapse has two major outcomes for the underlying crust hosting magma build-ups: 1) it drops some country-rock material towards the emptying magma body, and 2) it results in changes to the structure and the stress field of the shallowest upper crust (e.g. Corbi et al., 2015). An addition of pre-OTT roof material previously overlying the magma reservoir could explain a shift towards lower εHf, higher $^{87}Sr/^{86}Sr$ (Fig. 6), and $\delta^{18}O$ (Liu et al., 2022a) in the newly accumulating MTT magma which could now assimilate it. Little is known about the composition of such roof rocks at the time of OTT eruption, but the required materials would likely have been significantly older than the Quaternary Toba volcanics and either sedimentary or altered by meteoric water, such as, e.g., Palaeozoic to Miocene

(meta)sediments known from the caldera walls (Chesner and Rose, 1991). In this scenario, the initial addition of country rock would be progressively diluted over the following 600 ky by recharge addition of juvenile, high-εHf, low-$^{87}Sr/^{86}Sr$ melts that would bring it to the baseline isotopic value, and without any apparent effect of the later MTT evacuation and caldera collapse at 504 ka. However, in view of the clear changes in the locations of successive Toba calderas as proposed by Chesner and Rose (1991; Fig. 1A), we find a scenario of lateral shifts of the magma accumulation locus more likely (Fig. 7). Since successive caldera collapses affect the structure of the crust and its stress state, the restructuring of the shallow subsurface alone may facilitate preferential accumulation of magma in certain areas. We propose that following the large OTT caldera collapse in the SE sector of the present Toba caldera, the conditions for subsequent magma accumulation (MTT-YTT) were initially most favourable away from the former OTT magma body footprint, in the NW sector. As the magma storage region shifted, newly accumulated juvenile MTT magma interacted with different, fertile, older upper crust that had not been substantially modified by earlier Toba magmatism. This lower-εHf, higher-$^{87}Sr/^{86}Sr$ and likely high-$\delta^{18}O$ crust may have been assimilated until exhaustion of fertile assimilant material, or the locus of magma accumulation moved SE over time. Alternatively, the isotopic composition of MTT could reflect a change in deep melt source, whereby the shallow magma body was fed with melts that were more contaminated with low-εHf, high-$^{87}Sr/^{86}Sr$ and high-$\delta^{18}O$ materials either in the mantle wedge or lower crust (Liu et al., 2022b); however, we find it unlikely that the NW sector of Toba would experience such a drastic change in magma source character in the time between HDT and MTT eruptions. Instead, we propose that the departure of the MTT isotopic signature from the baseline has an upper-crustal origin. Given the final footprint of the YTT caldera, we find it most plausible that during the progressive growth of the giant YTT magma reservoir from NW to SE the balance of the newly accessed, older country rock to crust made up of Quaternary magmatic rocks (e.g. post-OTT mush/pluton) shifted gradually, resulting in fully buffered, Toba baseline-like isotopic compositions by 74 ka. The MTT eruption does not appear to have influenced this process; YTT magma evolved in full continuity with the magma erupted as MTT. That the YTT magma involved both materials similar to MTT in the NW sector and to OTT in the SE sector is further supported by YTT glass trace elements where distinct compositional endmembers have been shown to correspond to MTT and OTT-type magmas (Pearce et al., 2020). Such recycling of unerupted magmatic products from a continuum of crystal-dominated to melt-dominated domains within the sub-caldera crust is expected in long-lived caldera systems, and has been documented elsewhere using zircon age spectra (e.g. Charlier et al., 2005; Szymanowski et al., 2019). Shifts of magma storage areas between successive caldera-forming eruptions, such as the one seen here, have been inferred in several well-exposed caldera centres, typically based on changing caldera footprint position (Christiansen, 2001; Barker et al., 2021; Cas et al., 2022).

5.2.3. Development of shallow magma storage over the last 1.6 My

Time-resolved geochemical and isotopic fingerprinting of the Toba tuffs provides an opportunity to explore the evolution of the magmatic system over the last 1.6 My. Specifically, while we could not sample any intervening activity representing the inferred full range of compositions and eruptive styles, zircons from caldera-forming eruptions alone provide an integrated view of long-term trends in magma storage conditions.

The oldest available record of magmatic activity at Toba is represented by the Haranggaol andesite (not sampled here), which is stratigraphically older than the first large eruption of HDT but indistinguishable from it in *in situ* U–Pb zircon age, and thought to represent an early mafic-intermediate volcanic edifice (Chesner and Rose, 1991; Liu et al., 2022a,b). Closely following the andesites, HDT represents the first evolved-composition, explosive eruption of Toba. HDT is rhyolitic but is characterised by a pyroxene-rich mineral assemblage with scarce zircons that lack any substantial variability in composition while recording ca. 200 ky of crystallisation history (Fig. 4). Given the limited zircon compositional range (Fig. 5), as well as rounded zircon morphologies (Fig. S1), we interpret this to represent crystallisation close to zircon saturation, in conditions barely allowing zircon growth and possibly resulting in multiple growth-resorption cycles. Such conditions may be facilitated by growth and resorption of clinopyroxene, which may exert a strong control on zircon saturation conditions (Szymanowski et al., 2020). Considering the higher-T mineral assemblage without quartz and an indication of deeper storage (Fig. 6), the period leading to HDT eruption can be thought of as the first step in the development of a mature magma reservoir, with early, mid- to upper-crustal magma emplacement contributing to the thermal maturation of the crust and thus building a fertile ground for reservoir growth in the following period (Karakas et al., 2017).

In contrast, OTT, MTT and YTT are all high-silica rhyolites, and all contain abundant zircon. Single-crystal zircon trace element compositions (Fig. 5) testify to their formation in melts that were saturated in feldspar, zircon and allanite. Importantly, while large variations in zircon compositions imposed by the co-crystallising mineral phases are seen, no correlations between age and trace element variations are apparent (Fig. 4). This indicates that a large variety of melt compositions co-existed within the same upper-crustal magma reservoir, resulting in multiple co-erupted compositions of melts and minerals. This feature has been increasingly recognised in voluminous explosive rhyolites, and shown directly for YTT based on both proximal and distal glass compositions (Pearce et al., 2020), as well as for many other units worldwide, both in the simple framework of multiple co-erupted melt batches of discrete composition (Cooper et al., 2012; Ellis et al., 2014) and more complex geometries (Hildreth and Wilson, 2007; Szymanowski et al., 2019). The three youngest tuffs at Toba describe a similarly persistent heterogeneity over the time required for each magma accumulation (Fig. 4), both in composition and, by extension, amount of melt present. Reaching a high-crystallinity state indicated by the most extremely fractionated compositions may be key to allowing long-term storage of magma over extended timescales necessary for thermal maturation of the crust, which has been shown to be key to grow large magma reservoirs without erupting frequently (Forni et al., 2018; Townsend et al., 2019; Bouvet de Maisonneuve et al., 2021).

The age distribution (Fig. 4) shows near-continuous zircon crystallisation over the entire history of evolved magmatism at Toba, with only short breaks ($<$ ca. 100 ky in our data) that can either indicate lack of zircon saturation, or their locking into non-eruptible parts of the reservoir during early, post-caldera rebuilding stages. The remarkable continuity, and the corresponding large and constant variance of compositions, testify to stable magma supply conditions to the shallow Toba reservoir as a whole over at least 1.1 My (early OTT to YTT), which were not interrupted by the changes to the locus of new magma accumulation (Fig. 7). We believe that the persistence of magma supply centred over the same area for a prolonged time, favoured by the particular geodynamic setting, generated the key combination of warm, mature crust and the right magma flux to allow the growth of large magma bodies that peaked with the evacuation of >5000 km^3 of magma at 74 ka. Contrary to some other studies utilising similar methods (Wotzlaw et al., 2013; Szymanowski et al., 2019), we did not observe any long-term secular evolution or a rejuvenation trend prior to the caldera-forming events that could indicate the priming of the magma reservoir for eruption by decreasing magma crystal con-

tent. In fact, previous results for YTT have shown the opposite trend, that of increased complexity of the system before that eruption (Vazquez and Reid, 2004; Tierney et al., 2019). Overall, there is no clear indication in our data or that of other studies that the large eruptions at Toba can be linked to a change in magma supply.

6. Summary and outlook

We examined the four large caldera-forming eruptions of the Toba complex with high-precision zircon petrochronology, $^{40}Ar/^{39}Ar$ geochronology of feldspar, and glass and mineral chemistry. Zircon and melt compositions reflect early and deeper (>3 kbar) magma accumulation, likely within immature crust, prior to the eruption of Haranggaol Dacite Tuff at ca. 1.4 Ma, followed by complex, shallow (2–3 kbar) build-ups within a giant, mature magma reservoir that erupted as the Oldest (784 ka), Middle (504 ka) and Youngest Toba Tuff (74 ka). We show that magma reservoir conditions, and presumably the feeder magma fluxes, were relatively invariable over the studied period. Well-defined changes in Hf and Sr isotope compositions trace variations in the geometry of the magma reservoir and correlate to a major restructuring of the magma plumbing system in the aftermath of OTT caldera collapse.

After the major eruption of YTT that reshaped the caldera to produce the present-day lake-filled depression, Toba erupted a series of lava domes located close to the caldera rims and on the eastern flank of Samosir island. (U/Th)-He zircon ages indicate that post-collapse effusive activity started immediately after the YTT eruption and continued for ca. 6–24 ky (Mucek et al., 2017). The younger, western and southern domes are compositionally less evolved (andesites and dacites) than the older domes on Samosir that are similar in composition to the YTT (Chesner et al., 2020). This observation might indicate rebuilding of an upper crustal reservoir after the YTT eruption, which is supported by the existing geophysical data (Jaxybulatov et al., 2014). More geochemical and chronological work on these post-YTT magmas is critical to illuminate the current status and future evolution of the Toba caldera.

CRediT authorship contribution statement

Dawid Szymanowski: Writing – review & editing, Writing – original draft, Visualization, Methodology, Investigation, Conceptualization. **Francesca Forni:** Writing – review & editing, Writing – original draft, Visualization, Investigation, Conceptualization. **Marcus Phua:** Writing – review & editing, Writing – original draft, Investigation. **Brian Jicha:** Writing – review & editing, Writing – original draft, Investigation. **Daniel W.J. Lee:** Writing – review & editing, Investigation. **Ying-Jui Hsu:** Writing – review & editing, Investigation. **Hamdi Rifai:** Resources. **Blair Schoene:** Writing – review & editing, Funding acquisition. **Caroline Bouvet de Maisonneuve:** Writing – review & editing, Funding acquisition.

Declaration of competing interest

The authors declare that they have no known competing financial interests or personal relationships that could have appeared to influence the work reported in this paper.

Data availability

All analytical data are included in the online supplementary file.

Acknowledgements

This work was supported by the National Research Foundation, Singapore [grant NRF-NRFF2016-04] and the U.S. National Science Foundation [award EAR-1735512]. We thank Stefania Gili, Matthew Nadeau, and John Higgins for help with Hf analyses at Princeton. Jeffrey A. Oalmann and Rizaldi Putra are acknowledged for assistance during field work in Sumatra. We also thank Axel Schmitt, Jorge Vazquez, and two anonymous reviewers for comments that helped us improve the manuscript.

Appendix A. Supplementary material

Supplementary material related to this article can be found online at https://doi.org/10.1016/j.epsl.2023.118408.

References

Andersen, N.L., Jicha, B.R., Singer, B.S., Hildreth, W., 2017. Incremental heating of Bishop Tuff sanidine reveals preeruptive radiogenic Ar and rapid remobilization from cold storage. Proc. Natl. Acad. Sci. USA 114, 12407–12412.
Barber, A.J., Crow, M.J., Milsom, J., 2005. Sumatra: geology, resources and tectonic evolution. Geol. Soc. Lond. Mem. 31.
Barker, S.J., Wilson, C.J.N., Allan, A.S.R., Schipper, C.I., 2015. Fine-scale temporal recovery, reconstruction and evolution of a post-supereruption magmatic system. Contrib. Mineral. Petrol. 170, 1–40.
Barker, S.J., Wilson, C.J.N., Illsley-Kemp, F., Leonard, G.S., Mestel, E.R.H., Mauriohooho, K., Charlier, B.L.A., 2021. Taupō: an overview of New Zealand's youngest supervolcano. N.Z. J. Geol. Geophys. 64, 320–346.
Black, B.A., Lamarque, J.-F., Marsh, D.R., Schmidt, A., Bardeen, C.G., 2021. Global climate disruption and regional climate shelters after the Toba supereruption. Proc. Natl. Acad. Sci. USA 118, e2013046118.
Bouvet de Maisonneuve, C., Bergal-Kuvikas, O., 2020. Timing, magnitude and geochemistry of major Southeast Asian volcanic eruptions: identifying tephrochronologic markers. J. Quat. Sci. 35, 272–287.
Bouvet de Maisonneuve, C., Forni, F., Bachmann, O., 2021. Magma reservoir evolution during the build up to and recovery from caldera-forming eruptions–a generalizable model? Earth-Sci. Rev. 218, 103684.
Bouvier, A., Vervoort, J.D., Patchett, P.J., 2008. The Lu–Hf and Sm–Nd isotopic composition of CHUR: constraints from unequilibrated chondrites and implications for the bulk composition of terrestrial planets. Earth Planet. Sci. Lett. 273, 48–57.
Budd, D.A., Troll, V.R., Deegan, F.M., Jolis, E.M., Smith, V.C., Whitehouse, M.J., Harris, C., Freda, C., Hilton, D.R., Halldórsson, S.A., Bindeman, I.N., 2017. Magma reservoir dynamics at Toba caldera, Indonesia, recorded by oxygen isotope zoning in quartz. Sci. Rep. 7, 40624.
Cas, R.A.F., Wolff, J.A., Martí, J., Olin, P.H., Edgar, C.J., Pittari, A., Simmons, J.M., 2022. Tenerife, a complex end member of basaltic oceanic island volcanoes, with explosive polygenetic phonolitic calderas, and phonolitic-basaltic stratovolcanoes. Earth-Sci. Rev. 230, 103990.
Charlier, B., Wilson, C., Lowenstern, J., Blake, S., Van Calsteren, P., Davidson, J., 2005. Magma generation at a large, hyperactive silicic volcano (Taupo, New Zealand) revealed by U–Th and U–Pb systematics in zircons. J. Petrol. 46, 3–32.
Chesner, C., Rose, W.I., Deino, A., Drake, R., Westgate, J., 1991. Eruptive history of Earth's largest Quaternary caldera (Toba, Indonesia) clarified. Geology 19, 200–203.
Chesner, C.A., 1988. The Toba Tuffs and Caldera Complex, Sumatra, Indonesia: Insights into Magma Bodies and Eruptions. Michigan Technological University, Ann Arbor. 445 pp.
Chesner, C.A., 1998. Petrogenesis of the Toba Tuffs, Sumatra, Indonesia. J. Petrol. 39, 397–438.
Chesner, C.A., Barbee, O.A., McIntosh, W.C., 2020. The enigmatic origin and emplacement of the Samosir Island lava domes, Toba Caldera, Sumatra, Indonesia. Bull. Volcanol. 82, 1–20.
Chesner, C.A., Luhr, J.F., 2010. A melt inclusion study of the Toba Tuffs, Sumatra, Indonesia. J. Volcanol. Geotherm. Res. 197, 259–278.
Chesner, C.A., Rose, W.I., 1991. Stratigraphy of the Toba Tuffs and the evolution of the Toba Caldera Complex, Sumatra, Indonesia. Bull. Volcanol. 53, 343–356.
Christiansen, R.L., 2001. The Quaternary and Pliocene Yellowstone Plateau volcanic field of Wyoming, Idaho, and Montana. U.S. Geol. Surv. Prof. Paper 729-G.
Clemens, S.C., Kuhnt, W., LeVay, L.J., Anand, P., Ando, T., Bartol, M., Bolton, C.T., Ding, X., Gariboldi, K., Giosan, L., Hathorne, E.C., Huang, Y., Jaiswal, P., Kim, S., Kirkpatrick, J.B., Littler, K., Marino, G., Martinez, P., Naik, D., Peketi, A., Phillips, S.C., Robinson, M.M., Romero, O.E., Sagar, N., Taladay, K.B., Taylor, S.N., Thirumalai, K., Uramoto, G., Usui, Y., Wang, J., Yamamoto, M., Zhou, L., 2016. Site U1443. In: Clemens, S.C., Kuhnt, W., LeVay, L.J., the Expedition 353 Scientists (Eds.), Indian Monsoon Rainfall. Proceedings of the International Ocean Discovery Program 353. College Station, TX.

Cooper, G.F., Wilson, C.J.N., Millet, M.A., Baker, J.A., Smith, E.G.C., 2012. Systematic tapping of independent magma chambers during the 1 Ma Kidnappers supereruption. Earth Planet. Sci. Lett. 313–314, 23–33.
Corbi, F., Rivalta, E., Pinel, V., Maccaferri, F., Bagnardi, M., Acocella, V., 2015. How caldera collapse shapes the shallow emplacement and transfer of magma in active volcanoes. Earth Planet. Sci. Lett. 431, 287–293.
Costa, A., Smith, V.C., Macedonio, G., Matthews, N.E., 2014. The magnitude and impact of the Youngest Toba Tuff super-eruption. Front. Earth Sci. 2, 16.
Dehn, J., Farrell, J.W., Schmincke, H.-U., 1991. Neogene tephrochronology from Site 758 on northern Ninetyeast Ridge: Indonesian arc volcanism of the past 5 Ma. Proc. Ocean Drill. Program Sci. Results 121, 273–295.
Ellis, B.S., Bachmann, O., Wolff, J.A., 2014. Cumulate fragments in silicic ignimbrites: the case of the Snake River Plain. Geology 42, 431–434.
Fauzi, McCaffrey R., Wark, D., Prih Haryadi, P.Y., 1996. Lateral variation in slab orientation beneath Toba Caldera, northern Sumatra. Geophys. Res. Lett. 23, 443–446.
Forni, F., Degruyter, W., Bachmann, O., De Astis, G., Mollo, S., 2018. Long-term magmatic evolution reveals the beginning of a new caldera cycle at Campi Flegrei. Sci. Adv. 4, eaat9401.
Gao, M.-H., Liu, P.-P., Chung, S.-L., Li, Q.-L., Wang, B., Tian, W., Li, X.-H., Lee, H.-Y., 2022. Himalayan zircons resurface in Sumatran arc volcanoes through sediment recycling. Commun. Earth Environ. 3, 283.
Gasparon, M., Varne, R., 1998. Crustal assimilation versus subducted sediment input in west Sunda arc volcanics: an evaluation. Mineral. Petrol. 64, 89–117.
Hamilton, W.B., 1979. Tectonics of the Indonesian region. U.S. Geol. Surv. Prof. Paper 1078. 345 pp.
Hildreth, W., Wilson, C.J., 2007. Compositional zoning of the Bishop Tuff. J. Petrol. 48, 951–999.
Huber, C., Townsend, M., Degruyter, W., Bachmann, O., 2019. Optimal depth of subvolcanic magma chamber growth controlled by volatiles and crust rheology. Nat. Geosci. 12, 762–768.
Ito, H., 2020. Magmatic history of the Oldest Toba Tuff inferred from zircon U–Pb geochronology. Sci. Rep. 10, 17506.
Jaxybulatov, K., Shapiro, N., Koulakov, I., Mordret, A., Landès, M., Sens-Schönfelder, C., 2014. A large magmatic sill complex beneath the Toba caldera. Science 346, 617–619.
Jicha, B.R., Singer, B.S., Sobol, P., 2016. Re-evaluation of the ages of $^{40}Ar/^{39}Ar$ sanidine standards and supereruptions in the western US using a Noblesse multicollector mass spectrometer. Chem. Geol. 431, 54–66.
Jones, S., 1993. Mechanisms of Large Silicic Magma Chamber Zonation: the Youngest Toba Tuff, Sumatra. The Open University, UK.
Karakas, O., Degruyter, W., Bachmann, O., Dufek, J., 2017. Lifetime and size of shallow magma bodies controlled by crustal-scale magmatism. Nat. Geosci. 10, 446–450.
Keller, C.B., Schoene, B., Samperton, K.M., 2018. A stochastic sampling approach to zircon eruption age interpretation. Geochem. Perspect. Lett. 8, 31–35.
Klein, B.Z., Eddy, M.P., 2023. What's in an age? Calculation and interpretation of ages and durations from U-Pb zircon geochronology of igneous rocks. Geol. Soc. Am. Bull. https://doi.org/10.1130/B36686.1.
Knight, M.D., Walker, G.P., Ellwood, B.B., Diehl, J.F., 1986. Stratigraphy, paleomagnetism, and magnetic fabric of the Toba Tuffs: constraints on the sources and eruptive styles. J. Geophys. Res., Solid Earth 91, 10355–10382.
Kutterolf, S., Schindlbeck-Belo, J.C., Müller, F., Pank, K., Lee, H.-Y., Wang, K.-L., Schmitt, A.K., 2023. Revisiting the occurrence and distribution of Indian Ocean Tephra: Quaternary marine Toba ash inventory. J. Volcanol. Geotherm. Res. 441, 107879.
Lee, M.-Y., Chen, C.-H., Wei, K.-Y., Iizuka, Y., Carey, S., 2004. First Toba supereruption revival. Geology 32, 61–64.
Liu, P.-P., Caricchi, L., Chung, S.-L., Li, X.-H., Li, Q.-L., Zhou, M.-F., Lai, Y.-M., Ghani, A.A., Sihotang, T., Sheldrake, T.E., Simpson, G., 2021. Growth and thermal maturation of the Toba magma reservoir. Proc. Natl. Acad. Sci. USA 118, e2101695118.
Liu, P.-P., Chung, S.-L., Ma, B., Li, X.-H., Li, Q.-L., Lee, H.-Y., Zhang, X.-R., 2022a. Zircon Hf-O isotopic constraints on the origin and temporal evolution of the Toba volcanic system, Indonesia. Lithos 434–435, 106925.
Liu, P.P., Chung, S.L., Chesner, C.A., Gao, M.H., Lai, Y.M., Lee, H.Y., Yang, Y.H., 2022b. New insights into the petrogenesis of voluminous crustal-signature silicic volcanic rocks of the Toba eruptions (Indonesia). J. Geophys. Res., Solid Earth, e2022JB024559.
Mark, D.F., Petraglia, M., Smith, V.C., Morgan, L.E., Barfod, D.N., Ellis, B.S., Pearce, N.J., Pal, J.N., Korisettar, R., 2014. A high-precision $^{40}Ar/^{39}Ar$ age for the Young Toba Tuff and dating of ultra-distal tephra: forcing of Quaternary climate and implications for hominin occupation of India. Quat. Geochronol. 21, 90–103.
Mark, D.F., Renne, P.R., Dymock, R.C., Smith, V.C., Simon, J.I., Morgan, L.E., Staff, R.A., Ellis, B.S., Pearce, N.J., 2017. High-precision $^{40}Ar/^{39}Ar$ dating of Pleistocene tuffs and temporal anchoring of the Matuyama-Brunhes boundary. Quat. Geochronol. 39, 1–23.
Mason, B.G., Pyle, D.M., Oppenheimer, C., 2004. The size and frequency of the largest explosive eruptions on Earth. Bull. Volcanol. 66, 735–748.
Médard, E., Le Pennec, J.-L., 2022. Petrologic imaging of the magma reservoirs that feed large silicic eruptions. Lithos 428–429, 106812.
Min, K., Mundil, R., Renne, P.R., Ludwig, K.R., 2000. A test for systematic errors in $^{40}Ar/^{39}Ar$ geochronology through comparison with U/Pb analysis of a 1.1-Ga rhyolite. Geochim. Cosmochim. Acta 64, 73–98.
Mucek, A.E., Danišík, M., de Silva, S.L., Schmitt, A.K., Pratomo, I., Coble, M.A., 2017. Post-supereruption recovery at Toba Caldera. Nat. Commun. 8, 1–9.
Mucek, A.E., Danišík, M., de Silva, S.L., Miggins, D.P., Schmitt, A.K., Pratomo, I., Koppers, A., Gillespie, J., 2021. Resurgence initiation and subsolidus eruption of cold carapace of warm magma at Toba Caldera, Sumatra. Commun. Earth Environ. 2, 185.
Nishimura, S., Abe, E., Nishida, J.i., Yokoyama, T., Dharma, A., Hehanussa, P., Hehuwat, F., 1984. A gravity and volcanostratigraphic interpretation of the Lake Toba region, North Sumatra, Indonesia. Tectonophysics 109, 253–272.
O'Connor, L., Szymanowski, D., Eddy, M.P., Samperton, K.M., Schoene, B., 2022. A red bole zircon record of cryptic silicic volcanism in the Deccan Traps, India. Geology 50, 460–464.
Padilla, A.J., Gualda, G.A.R., 2016. Crystal-melt elemental partitioning in silicic magmatic systems: an example from the Peach Spring Tuff high-silica rhyolite, Southwest USA. Chem. Geol. 440, 326–344.
Page, B., Bennett, J., Cameron, N., Bridge, D.M., Jeffery, D., Keats, W., Thaib, J., 1979. A review of the main structural and magmatic features of northern Sumatra. J. Geol. Soc. 136, 569–577.
Pearce, N.J.G., Westgate, J.A., Gualda, G.A.R., Gatti, E., Muhammad, R.F., 2020. Tephra glass chemistry provides storage and discharge details of five magma reservoirs which fed the 75 ka Youngest Toba Tuff eruption, northern Sumatra. J. Quat. Sci. 35, 256–271.
Putirka, K., 2016. Amphibole thermometers and barometers for igneous systems and some implications for eruption mechanisms of felsic magmas at arc volcanoes. Am. Mineral. 101, 841–858.
Pyle, D.M., 1995. Mass and energy budgets of explosive volcanic eruptions. Geophys. Res. Lett. 22, 563–566.
Reid, M.R., Vazquez, J.A., 2017. Fitful and protracted magma assembly leading to a Giant eruption, Youngest Toba Tuff, Indonesia. Geochem. Geophys. Geosyst. 18, 156–177.
Rivera, T.A., Schmitz, M.D., Crowley, J.L., Storey, M., 2014. Rapid magma evolution constrained by zircon petrochronology and $^{40}Ar/^{39}Ar$ sanidine ages for the Huckleberry Ridge Tuff, Yellowstone, USA. Geology 42, 643–646.
Sakata, S., Hirakawa, S., Iwano, H., Danhara, T., Guillong, M., Hirata, T., 2017. A new approach for constraining the magnitude of initial disequilibrium in Quaternary zircons by coupled uranium and thorium decay series dating. Quat. Geochronol. 38, 1–12.
Schaltegger, U., Nowak, A., Ulianov, A., Fisher, C.M., Gerdes, A., Spikings, R., Whitehouse, M.J., Bindeman, I., Hanchar, J.M., Duff, J., 2019. Zircon petrochronology and $^{40}Ar/^{39}Ar$ thermochronology of the Adamello Intrusive Suite, N. Italy: monitoring the growth and decay of an incrementally assembled magmatic system. J. Petrol. 60, 701–722.
Schoene, B., Eddy, M.P., Samperton, K.M., Keller, C.B., Keller, G., Adatte, T., Khadri, S.F., 2019. U-Pb constraints on pulsed eruption of the Deccan Traps across the end-Cretaceous mass extinction. Science 363, 862–866.
Smith, V.C., Pearce, N.J.G., Matthews, N.E., Westgate, J.A., Petraglia, M.D., Haslam, M., Lane, C.S., Korisettar, R., Pal, J.N., 2011. Geochemical fingerprinting of the widespread Toba tephra using biotite compositions. Quat. Int. 246, 97–104.
Storck, J.-C., Wotzlaw, J.-F., Karakas, Ö., Brack, P., Gerdes, A., Ulmer, P., 2020. Hafnium isotopic record of mantle-crust interaction in an evolving continental magmatic system. Earth Planet. Sci. Lett. 535, 116100.
Szymanowski, D., Ellis, B.S., Wotzlaw, J.F., Bachmann, O., 2019. Maturation and rejuvenation of a silicic magma reservoir: high-resolution chronology of the Kneeling Nun Tuff. Earth Planet. Sci. Lett. 510, 103–115.
Szymanowski, D., Forni, F., Wolff, J.A., Ellis, B., 2020. Modulation of zircon solubility by crystal-melt dynamics. Geology 48, 798–802.
Tierney, C.R., Reid, M.R., Vazquez, J.A., Chesner, C.A., 2019. Diverse late-stage crystallization and storage conditions in melt domains from the Youngest Toba Tuff revealed by age and compositional heterogeneity in the last increment of accessory phase growth. Contrib. Mineral. Petrol. 174, 31.
Townsend, M., Huber, C., Degruyter, W., Bachmann, O., 2019. Magma chamber growth during intercaldera periods: insights from thermo-mechanical modeling with applications to Laguna del Maule, Campi Flegrei, Santorini, and Aso. Geochem. Geophys. Geosyst. 20, 1574–1591.
Turner, S., Foden, J., 2001. U, Th and Ra disequilibria, Sr, Nd and Pb isotope and trace element variations in Sunda arc lavas: predominance of a subducted sediment component. Contrib. Mineral. Petrol. 142, 43–57.
Vazquez, J.A., Reid, M.R., 2004. Probing the accumulation history of the voluminous Toba magma. Science 305, 991–994.
Weber, G., Blundy, J., 2023. A machine learning-based thermometer, barometer and hygrometer for magmatic liquids. EarthArXiv preprint. https://doi.org/10.31223/X5NW9P.
Wotzlaw, J.F., Schaltegger, U., Frick, D.A., Dungan, M.A., Gerdes, A., Günther, D., 2013. Tracking the evolution of large-volume silicic magma reservoirs from assembly to supereruption. Geology 41, 867–870.